Quasiparticle and γ-band structures in ^{156}Dy

S. Jehangir,[1,2] G. H. Bhat,[1,3,4] J. A. Sheikh,[1,4] S. Frauendorf,[5] S. N. T. Majola,[6,7] P. A. Ganai,[2] and J. F. Sharpey-Schafer[8]

[1]*Department of Physics, University of Kashmir, Srinagar 190 006, India*
[2]*Department of Physics, National Institute of Technology, Srinagar 190 006, India*
[3]*Department of Physics, Government Degree College Kulgam, Kashmir 192 231, India*
[4]*Cluster University Srinagar, Jammu and Kashmir 190 001, India*
[5]*Department of Physics, University of Notre Dame, Notre Dame, Indiana, USA*
[6]*iThemba LABS, National Research Foundation, P.O. Box 722, Somerset-West 7129, South Africa*
[7]*Department of Physics, University of Zululand, Private Bag X1001, Kwadlangezwa 3886, South Africa*
[8]*Department of Physics, University of the Western Cape, P.O. Box X17, Bellville 7535, South Africa*

(Received 18 October 2017; published 18 January 2018)

Excited band structures recently observed in ^{156}Dy are investigated using the microscopic triaxial projected shell model (TPSM) approach and the quasiparticle random phase approximation (QRPA) based on the rotating mean field. It is demonstrated that new observed excited bands, tracking the ground-state band, are the γ bands based on the excited two-quasineutron configurations as conjectured in the experimental work.

DOI: 10.1103/PhysRevC.97.014310

I. INTRODUCTION

A major challenge in nuclear theory is to elucidate the rich band structures observed in atomic nuclei [1]. The phenomenal progress achieved in experimental techniques in recent years has made it possible to probe nuclear structure properties at the extremes of spin and isospin. In some heavier nuclei, more than thirty band structures have been identified and some of these bands extend up to angular momentum of 60 [2–5]. The band structures provide valuable information on the dependence of nuclear properties on excitation energy and angular momentum. For instance, it is known that pairing correlations are reduced with angular momentum due to alignment of protons and neutrons in high-j intruder orbitals. The particles or quasiparticles in these high-j and low-Ω orbitals have maximum projection along the rotational axis and demand less collective rotation to generate the angular momentum. These quasiparticle (qp) configurations then become energetically favored and cross the ground-state configuration at a finite angular momentum, depending on the region.

In a more recent experimental study [6], the high-spin band structures in ^{156}Dy have been populated. The most interesting aspect of this investigation is the observation of the γ band based on the ground state up to highest angular momentum, $I = 32$, observed so far. The excited bands that decay to this γ band have been proposed to be the γ bands based on the two-quasiparticle configurations. This interesting proposition of the γ bands built on the quasiparticle excitations warrants investigations using theoretical approaches.

The γ band built on the ground-state or vacuum configuration was introduced by Bohr and Mottelson [1], who interpreted these $K^\pi = 2^+$ bands as a dynamic quadrupole deviation of the nuclear mean-field potential from the axial shape. In the framework of the unified model, it is considered an intrinsic excitation which, when combined with the rotational D function, restores the angular momentum. Several approaches have been developed to describe this intrinsic excitation in a microscopic way, including quasiparticle phonon [7,8], multiphonon [9–12], and dynamic deformation [13] models, and the quasiparticle random phase approximation (QRPA) based on the rotating mean field, which describes the γ bands based on high-spin yrast levels in a semiclassical way [14–20].

Recently, the microscopic approach of the triaxial projected shell model (TPSM) has been developed to describe the high-spin band structures in transitional nuclei [21–26]. In this approach, the three-dimensional projection method is applied to project out the good angular-momentum states from the triaxial intrinsic states. From the symmetry requirement, the projection from the self-conjugate vacuum state leads to even-K states with $K = 0,2,4,\ldots$. The $K = 0,2,4$ states represent the main components of the ground-state, γ, and $\gamma\gamma$ bands at low spin.

The TPSM approach includes multi-quasiparticle excitations, and it is evident from the very construction of the basis configurations that γ bands can be built also on the quasiparticle configurations. This interpretation is similar to the tidal wave approach, which will be applied to the γ vibration for the first time in this paper. It describes the γ vibration as a traveling wave, which corresponds to uniform rotation about the long axis of the triaxial shape. Using the cranking model, the properties of the γ vibration are calculated in a microscopic way without introducing any new parameters.

The recent experimental study of ^{156}Dy [6] provided evidence for the existence of a γ band based on the ground-state band up to very high spins and a second γ band, which is proposed to be built on the s configuration, which contains two rotational aligned $i_{13/2}$ quasineutrons. The purpose of the present work is to investigate the conjectured γ bands, based

on the quasiparticle excitations, using the TPSM approach as well as in the framework of the traditional approaches based on the rotating mean field.

As the band structures in ^{156}Dy have been observed up to spin $I = 32$, where four-quasiparticle configurations are expected to become important, four-neutron and four-proton quasiparticle configurations have been included for the first time in the TPSM basis. The paper is organized in the following manner: Section II A contains a brief description of the TPSM approach. Details can be found in our earlier publications [27–29]. The results obtained from the TPSM calculations are presented and compared with the experimental data in Sec. II B. In Sec. II C, the nature of γ bands is analyzed. Section III A discusses the structure of the positive parity bands in the complementary framework of the conventional cranked shell model and its relation to TPSM interpretation. Section III B reviews the application of the quasiparticle random phase approximation to the γ vibration in rotating nuclei from the earlier work in the literature. Section III C contains the tidal wave study of the γ vibration and discusses its relation to the TPSM. Conclusions are presented in Sec. IV.

II. TRIAXIAL PROJECTED SHELL MODEL APPROACH

A. Extension of the model

For even-even systems, the normal TPSM basis space consists of projected 0-qp or qp-vacuum, two-proton, two-neutron, and two-proton+two-neutron quasiparticle configurations. In the present investigation of the band structures in ^{156}Dy, high-spin states have been observed up to $I = 32$, and, in order to describe the states above $I = 20$ accurately, it is important to include also four-neutron and four-proton quasiparticle configurations. In the present work, we have extended the TPSM basis space to include these four-quasiparticle configurations, and the complete basis space employed in the present work is given by

$$\begin{aligned} &\hat{P}^I_{MK}|\Phi\rangle, \\ &\hat{P}^I_{MK}a^\dagger_{p_1}a^\dagger_{p_2}|\Phi\rangle, \\ &\hat{P}^I_{MK}a^\dagger_{n_1}a^\dagger_{n_2}|\Phi\rangle, \\ &\hat{P}^I_{MK}a^\dagger_{p_1}a^\dagger_{p_2}a^\dagger_{n_1}a^\dagger_{n_2}|\Phi\rangle, \\ &\hat{P}^I_{MK}a^\dagger_{n_1}a^\dagger_{n_2}a^\dagger_{n_3}a^\dagger_{n_4}|\Phi\rangle, \\ &\hat{P}^I_{MK}a^\dagger_{p_1}a^\dagger_{p_2}a^\dagger_{p_3}a^\dagger_{p_4}|\Phi\rangle, \end{aligned} \tag{1}$$

where $|\Phi\rangle$ is the vacuum state and the three-dimensional angular-momentum projection operator [30] is given by

$$\hat{P}^I_{MK} = \frac{2I+1}{8\pi^2}\int d\Omega\, D^I_{MK}(\Omega)\,\hat{R}(\Omega). \tag{2}$$

In the above equation, $\hat{R}(\Omega)$ is the rotational operator in terms of Euler angles. The adopted projected basis space in Eq. (1) is adequate enough to describe the high-spin states observed in ^{156}Dy up to $I = 32$. $|\Phi\rangle$ in the TPSM approach is the triaxial quasiparticle vacuum state, and the angular-momentum projection operator in Eq. (2) projects out not only the good angular momentum but also states having good K values. This is achieved by specifying a value for K in the rotational matrix, D, in Eq. (2).

It is worthwhile to mention that the basic strategy in TPSM is similar to that used in the spherical shell model (SSM) approach, except that now a deformed basis is employed rather than the spherical one. The deformed potential in TPSM provides an optimum basis to perform the spectroscopic studies of deformed heavier nuclei that are presently beyond the reach of the SSM approach. In the present work, Wick's theorem is used to evaluate the matrix elements of rotated many-quasiparticle states. This procedure becomes quite involved for more than two quasiparticles, and for identical four-quasiparticle states, considered in the present development, the number of terms in the Hamiltonian kernel is in the thousands. We are presently in the process of implementing the Pfaffian technique in the TPSM approach to include the higher quasiparticle states, as has been done recently in the PSM approach [31,32].

The projected basis of Eq. (1) is then used to diagonalize the shell model Hamiltonian. As in our earlier studies, we have employed the pairing plus quadrupole-quadrupole Hamiltonian [30,33–35]

$$\hat{H} = \hat{H}_0 - \frac{1}{2}\chi\sum_\mu \hat{Q}^\dagger_\mu\hat{Q}_\mu - G_M\hat{P}^\dagger\hat{P} - G_Q\sum_\mu \hat{P}^\dagger_\mu\hat{P}_\mu. \tag{3}$$

The QQ-force strength χ is adjusted such that the physical quadrupole deformation ϵ is obtained as a result of the self-consistent mean-field Hartree-Fock-Bogoliubov calculation [30]. The monopole pairing strength, G_M, is of the standard form

$$G_M = \left(G_1 \mp G_2\frac{N-Z}{A}\right)\frac{1}{A}\ (\text{MeV}), \tag{4}$$

where $-$ $(+)$ denotes neutron (proton). In the present calculation, we use $G_1 = 20.12$ and $G_2 = 13.13$, which approximately reproduce the observed odd-even mass difference in this region. This choice of G_M is appropriate for the single-particle space employed in the model, where three major shells are used for each type of nucleon ($N = 3,4,5$ for protons and $N = 4,5,6$ for neutrons). The quadrupole pairing strength G_Q is assumed to be proportional to G_M, with the proportionality constant being fixed as 0.16. These interaction strengths are consistent with those used earlier for the same mass region [27,30,36].

B. Comparison with experiment

TPSM calculations have been performed for ^{156}Dy by constructing the quasiparticle basis space with deformation parameters of $\epsilon = 0.278$ and $\epsilon' = 0.105$, which correspond to $\beta = 0.29$ and $\gamma = 20.6^\circ$ in the standard parametrization. The axial deformation parameter has been adopted from the earlier studies [37]. The nonaxial deformation parameter is chosen in such a way that the bandhead of the γ band is reproduced.

The angular-momentum projected energies from 0-qp, 2-qp, and 4-qp configurations, calculated with deformation parameters given above, are depicted in Fig. 1 for ^{156}Dy. The projection from 0-qp state results in $K = 0,2,4,\ldots$, with no odd values due to the symmetry requirement for the vacuum configuration, and gives rise to ground, γ, $\gamma\gamma$, ... bands. The

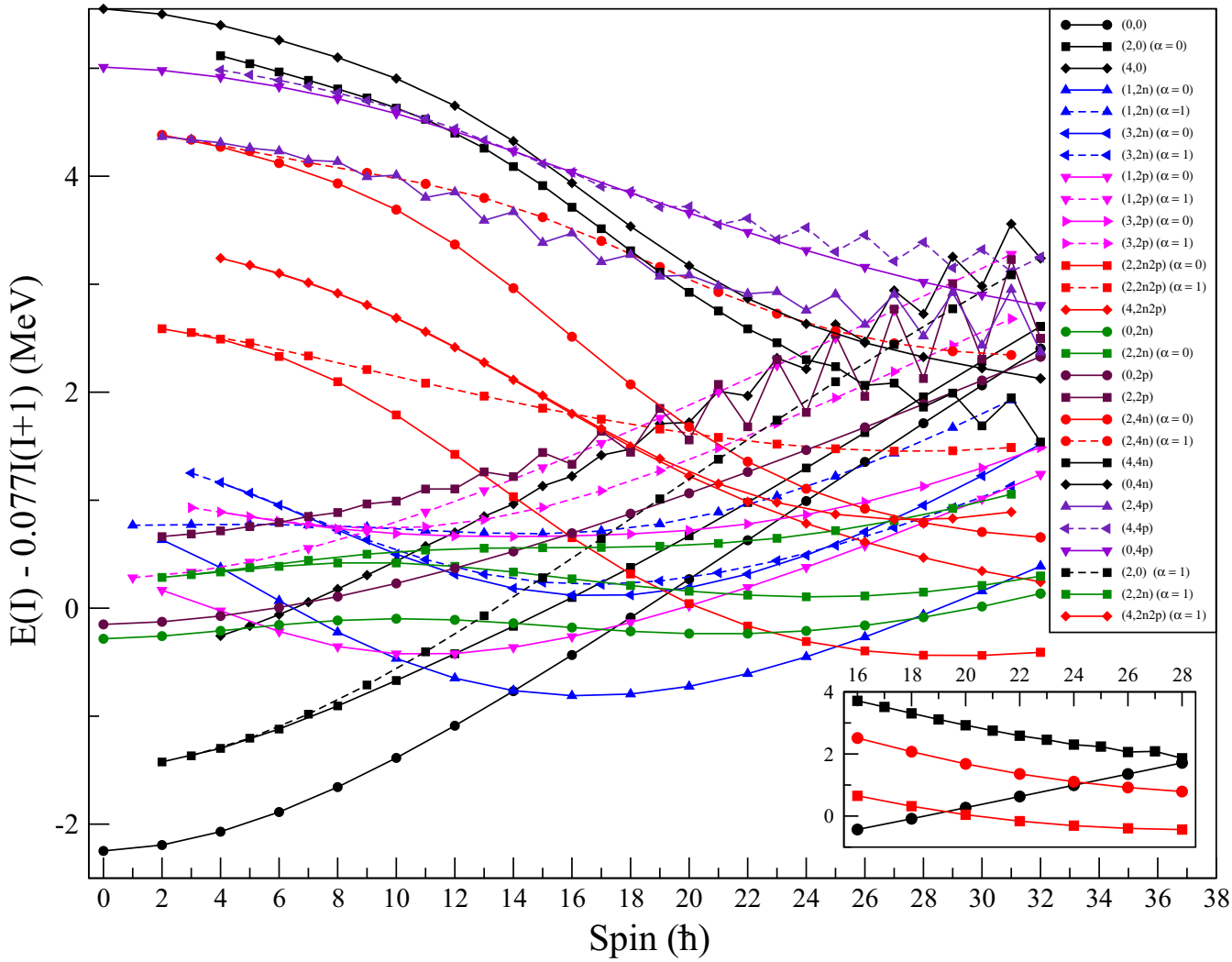

FIG. 1. TPSM projected energies, before band mixing, of positive parity states for ^{156}Dy. Bands are labeled as (K, qp numbers) so that the labels (0,0), (2,0), (4,0), (1,2n), (3,2n), (1,2p), (3,2p), (0,2n2p), (2,2n2p), and (4,2n2p) correspond to ground, γ, 2γ, two-neutron aligned state, γ band on this two-neutron aligned state, two-proton aligned state, γ-band on this two-proton aligned state, two-neutron plus two-proton aligned state, and γ and $\gamma\gamma$ bands built on this four-quasiparticle state. The excited $K = 0$ resulting from projection of two quasineutrons and two quasiprotons are denoted by (0,2n) and (0,2p), respectively. Some bands, having large signature splitting, are separated into even-spin (labeled as $\alpha = 0$) and odd-spin states (labeled as $\alpha = 1$). The first crossing at $I = 14$ is due to the (1,2n) aligned configuration that forms the s-band configuration. The second and third crossings at about $I = 24$ and 28 are due to the aligning 4n configurations with $K = 2$ and 4, respectively. The inset depicts the four-quasiparticle crossings with the ground-state band.

bandhead of the γ band is at an excitation energy of 0.98 MeV from the ground state and the $\gamma\gamma$ band lies at 2.13 MeV.

Figure 1 illustrates how the nonrotating quasiparticle basis states of the TPSM become entangled with increasing angular momentum. The ground-state band is crossed by the signature, $\alpha = 0$ branch of the (1,2n) band, which is a two-quasineutron aligned configuration having $K = 1$, at $I = 14$. Further, the $\alpha = 0$ component of the two-quasiproton aligned band, (1,2p), with $K = 1$ also crosses the ground-state band at $I = 18$. There are also crossings in the excited configuration; for instance, the γ band built on the two-quasineutron configuration (3,2n) having $K = 3$ crosses the normal γ band at $I = 17$. In fact, the lowest odd-spin states in the spin range $I = 17$–25 originate from this configuration. For spin above $I = 26$, we note that four-quasiparticle states (2,2n2p) become yrast. In Fig. 1, the lowest projected $K = 0$ bands, resulting from two-neutron and two-proton quasiparticle structures, are also plotted. These two bands are almost degenerate for low-spin states, with bandheads at about 2 MeV excitation energy. For high-spin states, however, the $K = 0$ two-quasineutron state becomes favored.

The projected bands from four-neutron and four-proton quasiparticle configurations are also plotted in Fig. 1 and the band structures obtained from these states lie at a higher excitation energy compared to two-neutron+two-proton quasiparticle bands. As is evident from the figure, these configurations remain higher in energy. However, it is noted that the $\alpha = 0$ component of the four-neutron quasiparticle state, having $K = 2$, crosses the ground-state band at $I =$ 24. The projected band from the $K = 4$ component of the

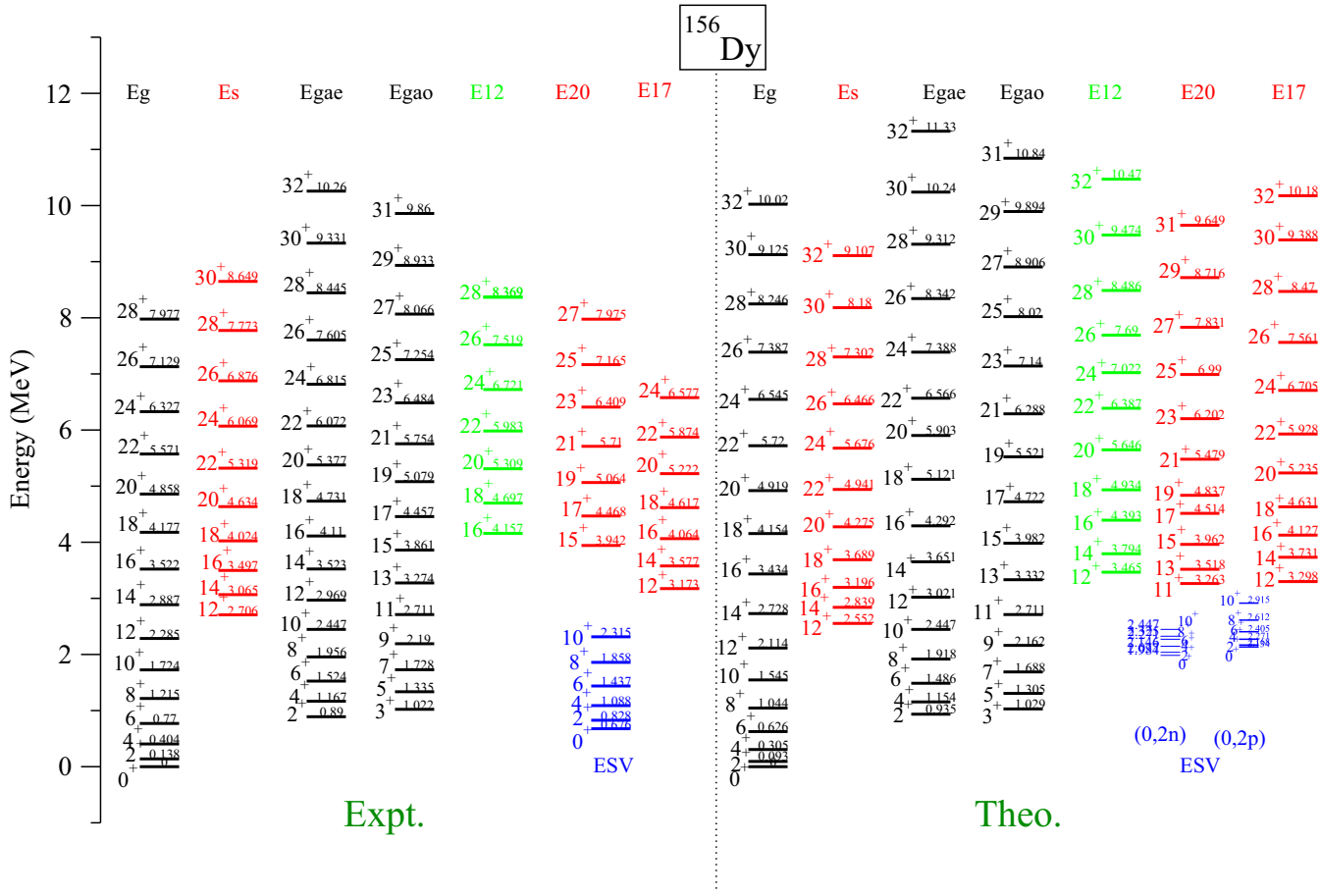

FIG. 2. Comparison of the measured positive parity energy levels of the ^{156}Dy nucleus [6] and the results of TPSM calculations.

four-neutron state also crosses the ground-state band at a higher spin value. On the other hand, the $\alpha = 1$ branch of this configuration and also the four-proton quasiparticle band structures lie at higher excitation energies and do not cross the ground-state band up to the highest studied spin value.

In the next stage of the TPSM study, the lowest projected states, shown in Fig. 1, and many more (∼130 for each angular momentum) are employed to diagonalize the shell model Hamiltonian, Eq. (3). The energies obtained after diagonalization are compared with the measured data in Figs. 2 and 3. The bands are labeled as in the experimental work [6]. The association between the calculated and experimental bands is discussed below. In Fig. 2, we provide the exact energies that can be used for further investigations. Figure 3 demonstrates that the TPSM calculations describe well the structure of the yrast region. However, the calculated spectrum is too spread out in energy. As discussed in Sec. II A, this is probably a consequence of the deformation and the pair gaps being kept constant.

To have a closer comparison between theory and experiment, the excitation energies are reduced by the rotor contribution, and the resulting energies are displayed in Fig. 3 [bottom panels (e) and (f)]. It is evident from the two figures that TPSM reproduces the experimental data quite reasonably with the exception of the excited 0^+ band referred to as the SV band. The bandhead of the experimentally observed band is at 0.7 MeV excitation and the predicted neutron excited 0^+ is at about 1.9 MeV. Theoretically, it is expected to lie at about 2 MeV, which is equal to the excitation energy of the two-quasiparticle states as is evident from Fig. 2. There are some extra correlations, not included in the present work, that bring it down to 0.7 MeV and clearly it is of considerable interest to investigate this problem in detail. It may be of vibrational type, a pairing isomer, or a shape coexisting structure. The TPSM does not include corrections of this type.

The correspondence between the theoretical and the experimental band structures plotted in Figs. 2 and 3 is made through the wave function analysis as discussed in the following. For some bands, it was possible to identify a few lower angular-momentum states, not observed in the experimental data, through this wave function analysis. The dominant components of the wave functions of the band structures are depicted in Fig. 4. The ground-state band, shown in the top panel of this figure, has up to $I = 14$ the largest component of (0,0), which is the $K = 0$ projected state from the triaxial vacuum configuration. It is also evident that the two-quasiproton component, $(1,2p)$, is building up with spin and becomes dominant in the spin region $I = 18$–22. For $I =$ 24 and beyond, four-quasiparticle components are becoming important, in particular the $K = 2$ four-neutron configuration. Therefore, this band is not really the ground-state band as it

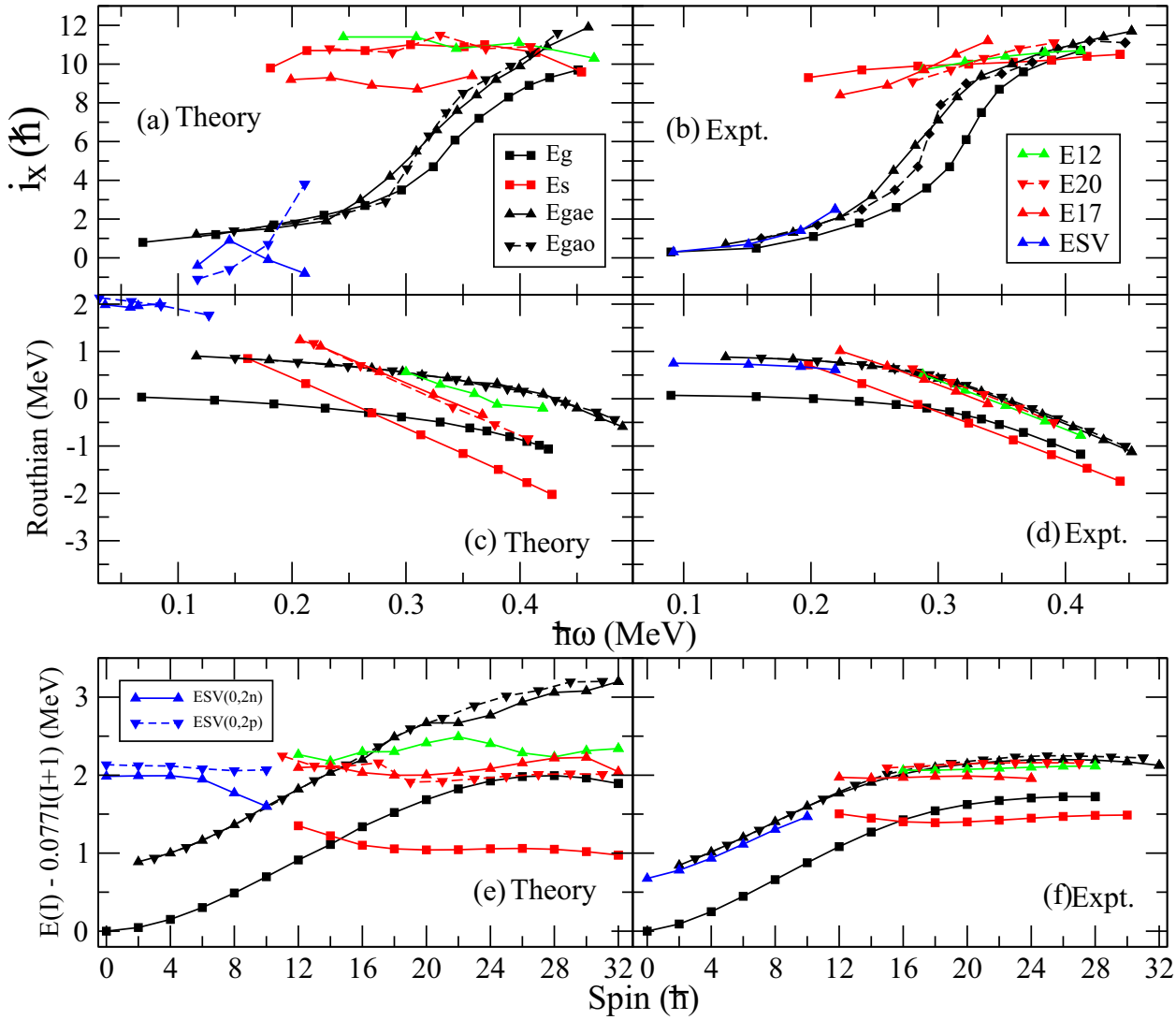

FIG. 3. Experimental energies (right panel) of the positive parity bands in ^{156}Dy as reported in Fig. 4 of Ref. [6] compared with the TPSM calculations (left panel). Labeling: Eg - ground-state band, Es - s band, Egae - even-spin γ-band, Egao - odd-spin γ band, ESV - SV band, E12 - band 12, E17 - band 17, E20 - band 20. Even-spin states are connected by solid lines, odd-spin states by dashed lines. In the upper panel $I_{\rm ref} = \omega\,\mathcal{J}_0 + \omega^3\,\mathcal{J}_1$ is subtracted. In the lower panel $E'_{\rm ref} = -\omega^2\,\mathcal{J}_0/2 - \omega^4\,\mathcal{J}_1/4$ is subtracted with $\mathcal{J}_0 = 23\ \hbar^2{\rm MeV}^{-1}$ and $\mathcal{J}_1 = 90\ \hbar^4{\rm MeV}^{-3}$.

has dominant two-quasiparticle and four-quasiparticle configurations for $I = 18$ and beyond. The wave function of the s band, shown in the second panel of Fig. 4, has the largest component from the aligned two-quasineutron state, $(1,2n)$, up to $I = 24$, and beyond this spin value the four-quasiparticle configurations dominate.

The largest component in the wave function of the even-spin γ band, shown in the third panel of Fig. 4, up to $I = 14$ is $(2,0)$, which is the $K = 2$ projected state from the 0-qp configuration. It is also noted that the component $(3,2p)$, which is the γ band built on the two-proton aligned band, is quite large in spin regime $I = 14$–18, and above $I = 18$ the s-band configuration, $(1,2n)$, becomes dominant. For the odd-spin γ band, the composition of the wave function is similar to the even-spin branch. Bands 17 and 20, shown in the fifth and sixth panels of Fig. 4, have interesting structures with the dominant component from $(3,2n)$, which is the γ band based on the two-quasineutron configuration.

From the above analysis, the emerging picture for the band structures labeled as 17 and 20 is quite similar to what has been proposed in the experimental work [6]. The component $(3,2n)$, which is the γ band built on the two-neutron aligned configuration, is quite dominant in the wave functions of the band structures labeled as band 17 and band 20. These bands are built on the same intrinsic quasiparticle as that of the s band of the second panel in Fig. 4, except that these are projected with $K = 3$. It is also evident from Fig. 4 that these are not purely γ bands built on the two-quasineutron configuration as these also have significant contributions from other configurations. This is related to the inter-band mixing, in particular for high-spin states and also due to nonorthogonality of the projected states.

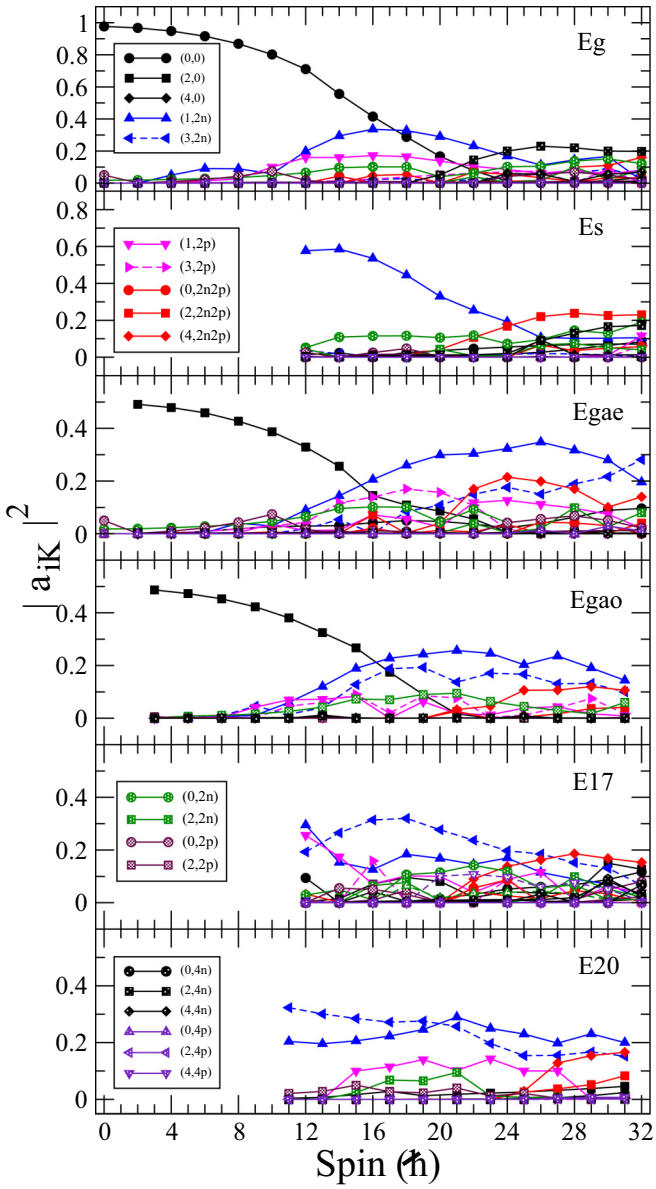

FIG. 4. Probability of various projected K configurations in the wave functions of the band structures after diagonalization are plotted for the ^{156}Dy nucleus.

Further, it is interesting to note from Fig. 4 that the even and odd γ-bands initially have the dominant component (2,0) as expected; however, for intermediate spin values the configuration $(3,2p)$ becomes important, which is similar to the ground-state band. This has to be the case, otherwise the γ band would not track the ground-state band. This configuration is the γ band built on the two-quasiproton configuration. The ground-state band is crossed by the normal two-quasiproton configuration and we infer from Fig. 4 that, for the γ band, it is γ band based on the two-quasiproton state that crosses.

The experimental interpretation of the band structures as γ bands built on the ground-state and two-quasiparticle configurations is based on the transition probabilities between the bands. The transition probabilities have been calculated in the TPSM approach with the effective charges of $1.5e$ for protons and $0.5e$ for neutrons. The $B(E2)$ values for the transition between the ground state and the s bands are depicted in Fig. 5 along with the known experimental values. Two dips in the $B(E2)$ curve for the ground-state band are due to the crossing of the two-proton and four-neutron aligned configurations at spins $I = 18\hbar$ and $24\hbar$, respectively. A small drop in the $B(E2)$ transitions of the s band at $I = 14\hbar$ is due to mixing of $(2,2n)$ and ground-state bands. Further, as in the experimental work, we have also evaluated the ratios R_{E2} of the out-of-band $B(E2;\text{out})$ to the in-band $B(E2;\text{in})$ strengths, where the out-of-band transitions connect the γ band with the ground-state band and bands 17 and 20 with the s band. [It needs to be added that $B(M1)$ transition probabilities, shown in Table I, are an order of magnitude smaller than $B(E2)$ transitions and hence evaluation of branching ratios

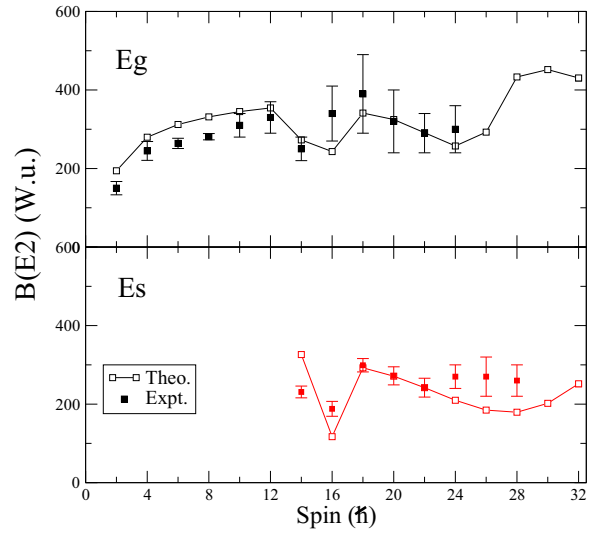

FIG. 5. Calculated $B(E2)$ transition probabilities for the ground-state band and the s band using the TPSM approach. The experimental values have been taken from Refs. [38–40].

TABLE I. Calculated $M1$ (μ_N^2) units from Egao → Eg and E20 → Es of the ^{156}Dy nucleus.

Spin (I^π)	Egao → Eg	E20 → Es
3^+	0.013	
5^+	0.011	
7^+	0.010	
9^+	0.008	
11^+	0.003	
13^+	0.002	0.124
15^+	0.004	0.122
17^+	0.006	0.071
19^+	0.008	0.029
21^+	0.002	0.017
23^+	0.003	0.009
25^+	0.005	0.005
27^+	0.003	0.007
29^+	0.004	0.001
31^+	0.001	0.002

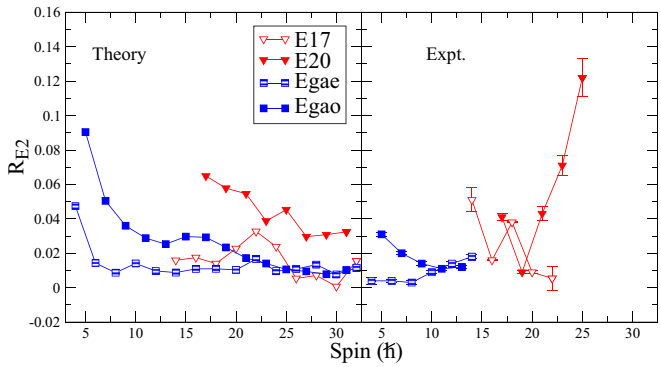

FIG. 6. Ratios of the $B(E2)$ values for out-of-band to in-band transitions $R_{E2} = B(E2;\text{out})/B(E2;\text{in})$ for the γ decays from the γ band to the ground-state band and for the γ decays from bands 17 and 20 to the s band

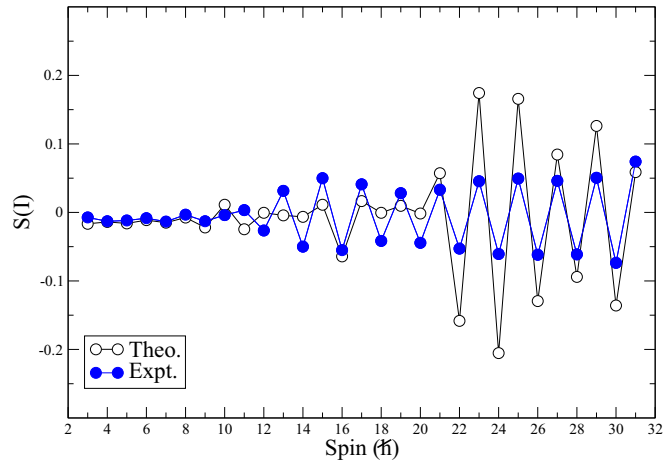

FIG. 7. Comparison of observed and TPSM calculated staggering parameter, Eq. (5), for the γ band in ^{156}Dy.

with $B(E2)$ values only is justified.] As depicted in Fig. 6, the R_{E2} values for all the bands are of same order of magnitude, supporting the interpretation that bands 17 and 20 are the γ bands built on the s-band configuration. The TPSM reproduces fairly well the experimental values.

The wave function of band 12 for spin states of $I = 16$, 18, and 20 are dominated by the two-proton aligned configuration, $(1,2p)$, and above $I = 24$ the wave function has a predominant contribution from four-quasiparticle states. Clearly, g-factor measurements are needed to probe the intrinsic structures of these band structures.

To examine further the quasiparticle structures of the observed band structures, we have analyzed the alignments of the bands as a function of the rotational frequency, and the results are presented in Fig. 3 [top panels (a) and (b)]. The observed ground-state band has a gradual increase in the alignment at a rotational frequency of $\hbar\omega = 0.3$ MeV. This increase is also noted in the TPSM calculated alignment, although it is slower than in the experimental data. This increase can be traced to the alignment of four neutrons having $K = 2$. This configuration crosses the ground-state band at $I = 24$ and becomes the dominant component in the ground-state band above this spin value, as is evident from Fig. 4. Both even- and odd-spin members of the γ band also show an increase in the aligned angular-momentum, which is due to the increasing contribution of $(1,2n)$ component in these band structures.

C. Nature of the γ bands

Analyzing the collective Bohr-Hamiltonian results, it has been suggested that signature splitting of the γ band is sensitive to the nature of γ deformation (see, e.g., the review [41]). The observed pattern is as follows: for harmonic γ vibration about an axial shape, both signatures are degenerate; for a γ-independent potential, even spin is below odd spin; for a rigid triaxial potential, odd spin is below even spin. To quantify the tendency, the following staggering parameter has been introduced:

$$S(I) = \frac{E(I) - [E(I-1) + E(I+1)]/2}{E(2_1^+)}, \qquad (5)$$

which measures the energy of state I relative to the average energy of the two neighbours. Figure 7 compares the TPSM results with experiment for the γ band on top of the ground-state band. The staggering $S(I)$ is quite small at low spin, which is expected for a well established axial shape. Above $I = 10$ the staggering increases, with the even-spin states below the odd ones. The TPSM calculations reproduce the observed staggering pattern, as well as the $R_{E2} = B(E2;\text{out})/B(E2;\text{in})$ values, as shown in Fig. 6 and, therefore they account for the nature of the γ deformation of ^{156}Dy nucleus. The even spin being lower, which is a signature for γ softness, appears to be in conflict with the assumption of the TPSM of a fixed γ deformation, which suggests that the criterion based on the Bohr Hamiltonian does not apply for $I > 10$ as the TSPM ratios R_{E2} are consistent with experiment. Within the TPSM framework, the staggering pattern can be related to the following: for low even-spin states the major components are $(2,0)$ and $(2,2p)$. The two-neutron aligned configuration, $(1,2n)$, becomes important above $I = 10$, as is evident from Fig. 4, showing the wave function probabilities. For the even-spin members of the γ band, the low-energy even-spin states $(1,2n)$ $(\alpha = 0)$ (cf. Fig. 1) have a large probability. For the odd-spin members of the γ band the high-energy odd-spin states $(1,2n)$ $(\alpha = 1)$ (cf. Fig. 1) have a large probability.

Bands 17 and 20 are assigned to the even- and odd-spin members of the γ band on top of the s configuration because the basis states $(3,2n)$ $(\alpha = 0,1)$ are dominant, where both signatures have nearly the same energy (cf. Fig. 1). As for the γ band on top of the ground-state band, both signatures contain a large $(1,2n)$ component of the respective signature, which energetically prefers the even-spin members.

As seen in Fig. 4, the γ-bands are distributed over multiple basis states. As we shall discuss in the next section, the QRPA treatment of the γ vibration based on the s band indicates substantial fragmentation as well. Another reason is the change of the quasiparticle structure caused by rotation. Since the TPSM uses the quasiparticle configurations in the nonrotational potential as a basis, it describes the modification

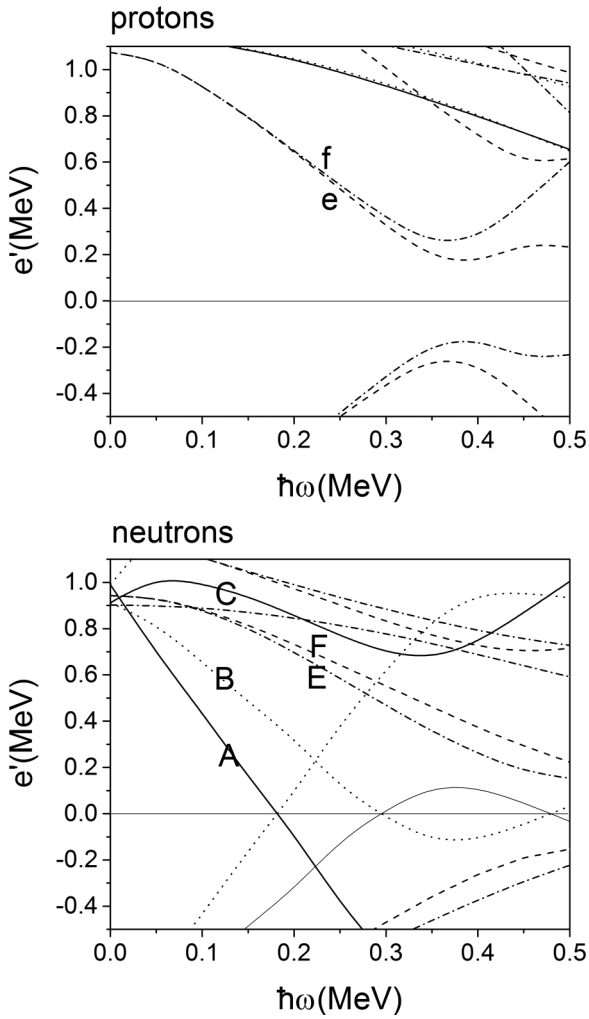

FIG. 8. Quasiparticle Routhians for ^{156}Dy.

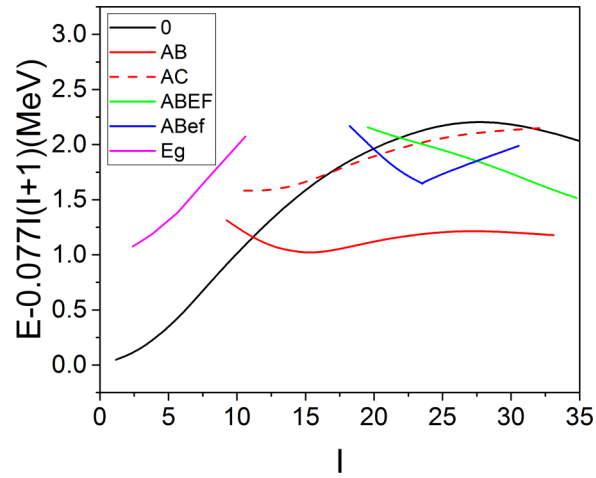

FIG. 9. Energies of the lowest positive parity bands in ^{156}Dy calculated by means of the cranking model. The bands are labeled by the occupied quasiparticles in Fig. 8. "Eg" is the γ band calculated by means of the tidal wave approach. Even-spin states are connected by straight lines, odd-spin states by dashed lines.

of the quasiparticle structure in the rotating potential by mixing the nonrotating configurations.

III. ROTATING MEAN-FIELD INTERPRETATION

A. Cranked shell model

Fig. 2 displays the experimental energies and Fig. 3 the experimental aligned angular momenta and Routhians for the positive parity bands. The simplest-possible interpretation is the cranked shell model (CSM) [42], which associates the bands with quasiparticle configurations in a potential rotating with frequency $\hbar\omega$ about one of its principal axes. Figure 8 depicts a calculation using the axial Nilsson potential combined with the monopole pair field as described in Ref. [42]. The deformation parameters are $\varepsilon = 0.26$ and $\gamma = 0$, which are close to the equilibrium deformation found by means of the cranked Nilsson-Strutinsky method for the relevant spin range [4]. The pair gaps are $\Delta_p = 1.0$ MeV and $\Delta_n = 0.9$ MeV. The ground-state band is represented by the vacuum, denoted by 0. Below $\hbar\omega = 0.15$ MeV, it corresponds to all negative-energy quasiparticle Routhians being occupied. Above, it corresponds to the adiabatic continuation of this configuration. The other configurations are denoted by the occupied Routhians labeled by the letters (the reflected-through-0 Routhians are unoccupied).

Figures 9 and 10 show the lowest positive parity bands labeled by their quasiparticle configurations. Comparing the CSM calculation with the experiment shown in Figs. 2 and 3, one notices that the crossing between the g band (configuration 0) and the s bands (AB) is qualitatively described. The CSM crossing frequency of $\hbar\omega = 0.23$ MeV underestimates the experimental value of $\hbar\omega = 0.28$ MeV, which is a well known deficiency of the CSM. The aligned angular momenta are of the right magnitude. The distance between the two bands after their crossing is overestimated (about 1 MeV in experiment vs about 2 MeV in the calculation). We attribute this to the assumption of a fixed deformation and fixed pairing gaps. The cranked Nilsson-Strutinsky calculations of Ref. [4], which assume no pairing and optimize the deformation for each configuration, obtain a more compressed spectrum, close to experiment. The CSM gives two even-spin (ABEF and ABef) bands and one odd-spin (AC) band between the s and the g bands, where Ref. [6] suggests the experimental location of the two signatures of the γ band on top of the s band. The close neighborhood may cause fragmentation of the collective strength among these two-quasiparticle (relative to AB) excitations.

B. Quasiparticle random phase approximation

The quasiparticle random phase approximation is the standard extension of the mean-field approximation to describe collective excitations. In order to describe the γ vibrations in rotational nuclei, the authors of Refs. [14–20] applied QRPA to the rotating mean-field and the pairing + quadrupole quadrupole model Hamiltonian, Eq. (3), with $G_Q = 0$. Since the rotating mean-field conserves signature, the QRPA leads to

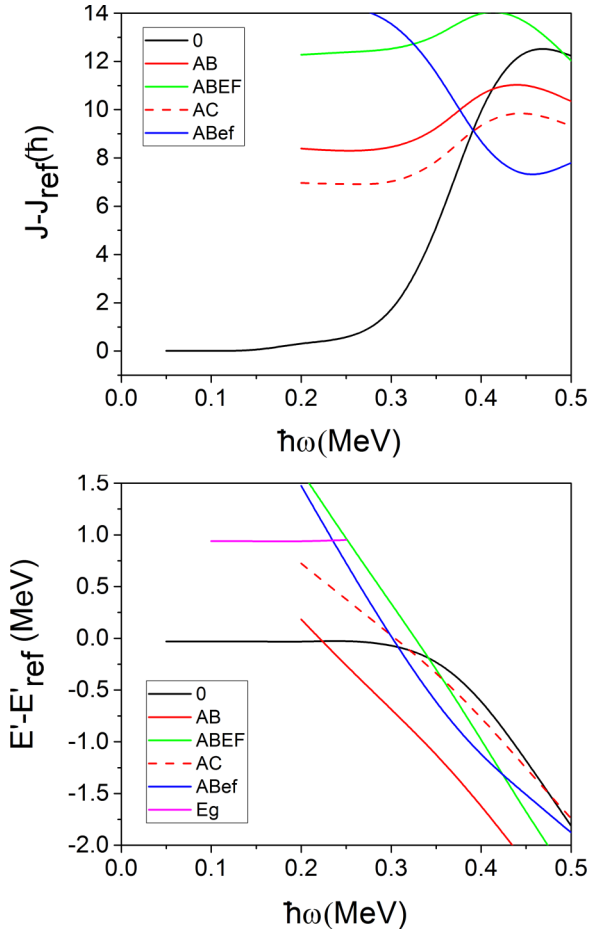

FIG. 10. Upper panel: Angular-momentum expectation values calculated by means of the cranking model relative to the reference. Lower panel: Routhians relative to the reference. Reference as in Fig. 3.

two independent sets of equations: one for even and the other one for odd spins.

Figure 11 shows the QRPA results of Refs. [18–20]. The authors used the self-consistency requirement for a harmonic oscillator potential and volume conservation introduced by Bohr and Mottelson [1] to determine the quadrupole deformation and to fix the coupling constant χ. The calculations reproduce very well the experimental energies of the odd-spin branch of the γ band on top of the g band. The calculated branching ratios $R_{E2} = B(E2, I \to I-1\,\text{:out})/B(E2, I \to I-2\,\text{:in}) \sim 0.02$ between the transitions out of and within the γ band account for the measured ratios [6] (see Fig. 6). Above the crossing between the g and s bands (g band stands for the ground-state band and s band stands for the two-quasiparticle aligned band), the QRPA solutions are based on the ss band, which is yrast. The three lowest odd-spin solutions are found close together. This suggests that the collective vibrational strength may be fragmented over these states instead of being concentrated in one individual state. The authors quote only the ratio $B(E2, I \to I-1\,\text{:out})/B(E2, I \to I-2\,\text{:in}) \sim 0.04$ for the lowest band. The value is consistent with the widely scattered experimental ratios of band 20 (see Fig. 6), whose

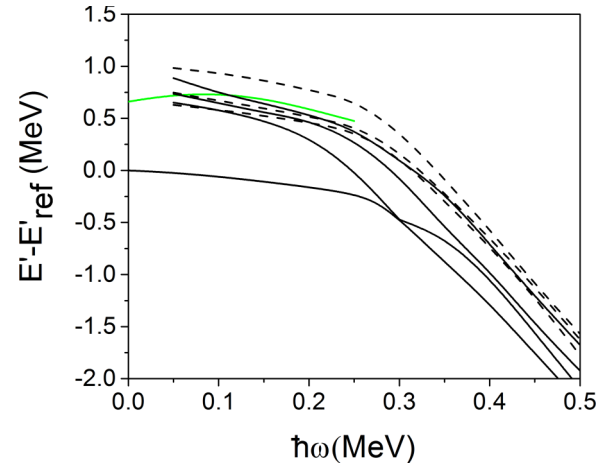

FIG. 11. Routhians of the lowest positive parity bands in ^{156}Dy calculated by means of the QRPA extension of the rotating mean-field derived from the pairing + quadrupole quadrupole model Hamiltonian. Even-spin states are connected by straight lines, odd-spin states by dashed lines. The green line depicts the QRPA results for the β band, i.e., the band based on the 0_2^+ state. The figure was prepared using the results of Refs. [18–20]. Reference energy is as in Fig. 3.

excitation energy with respect to the s band of about 0.75 MeV is somewhat larger than the QRPA value of about 0.60 MeV. The lowest three even-spin QRPA solutions are close together as well, which may lead to fragmentation. The lowest solution lies about 0.2 MeV above yrast, which is substantially lower than the position of band 17, the experimental candidate for the even-spin γ band. The calculated ratio $B(E2, I \to I-2\,\text{:out})/B(E2, I \to I-2\,\text{:in}) \sim 0.01$ is to be compared with the experimental ratio $\sim$0.2.

The QRPA approach becomes unreliable in the vicinity of the crossing of the g and s bands. The reason is that g and s configurations have different deformations (0 axial and AB triaxial). The cranking model produces a mixing between the configurations, which makes the even-spin QRPA energy approach zero, which is an artifact. The mixing falsifies the energies of the lowest QRPA even-spin solution already away from the crossing. In contrast to experiment, the even-spin solution (not shown) was found below the odd-spin sequence. The low energies of the even-spin QRPA solutions on top of the s configuration may be an artifact as well. The authors of Refs. [14–17] avoided these problems by removing the mixing between the g and s configurations. For the studied nucleus ^{164}Er both the even-spin and odd-spin QRPA solutions are stable in the crossing region.

As seen in Fig. 11, The QRPA calculations [20] reproduce the experimental energies of the SV band very well. The structure of the QRPA solution is not analyzed in detail. By construction, it has to be a combination of a β-type and a pairing vibration.

C. Tidal wave approach

The tidal wave concept has been developed to describe the yrast sequence of near-spherical and transitional nuclei [43,44]. It can be directly applied to the γ degree of freedom.

The γ vibration carries $2\hbar$ of angular-momentum along the symmetry axis. Classically, the sequence $n = 1,2,3,\ldots$ of aligned γ phonons is represented by a wave traveling around the symmetry axis 3 with the angular velocity $\hbar\omega_\gamma = E_\gamma/2$ carrying the angular-momentum $J_3 = K\hbar = 2n\hbar$. In the co-rotating frame, the wave is represented by a constant γ deformation, which increases $\propto \sqrt{n}$. For a traveling wave the angular momentum and energy increase by increasing the amplitude while the rotational frequency stays constant. For a triaxial rotor the states above the yrast sequence are also generated by adding quanta of angular momentum along the axis with the smallest moment of inertia. The difference to the tidal wave is that the angular momentum and energy increase by increasing the rotational frequency while the deformation stays constant. Obviously, the concept also applies to the intermediate cases of an anharmonic γ vibration and a soft triaxial rotor.

It is important to realize that it is not possible to distinguish between a triaxial rotor and a harmonic γ vibration, as long as one considers only the first excited ($K = 2$) band. In both cases an angular momentum of $J_3 = 2\hbar$ is generated by a γ-deformed shape rotating about the 3-axis. To differentiate, one has to take the next ($K = 4$) band into consideration. The K dependence of ω_γ is indicated by the level distance, $\hbar\omega_\gamma = [E_\gamma(K) - E_\gamma(K-2)]/2$. In the case of a vibration, the level distance is the same and so is the frequency ω_γ for $K = 2$ and $K = 4$ bands. To view it as a rotation, $\omega_\gamma = K/\mathcal{J}$ implies $\mathcal{J}(K = 4) = 2\,\mathcal{J}(K = 2)$. Because $\mathcal{J} \propto \gamma$, one must have deformation parameter $\gamma(K = 4) = \sqrt{2}\gamma(K = 2)$, which means $E_\gamma(K = 4) = 2E_\gamma(K = 2)$. In the case of the rigid triaxial rotor, $\gamma(K = 4) = \gamma(K = 2)$, and, with a fixed moment of inertia $\mathcal{J}$, the energy $E_\gamma = K^2/2\mathcal{J}$, which means that $\omega_\gamma(K = 4) = 2\omega_\gamma(K = 2)$ implying $E_\gamma(K = 4) = 4E_\gamma(K = 2)$. This explains why the TPSM approach [27] which operates with a fixed γ deformation describes the first excitations of γ vibrational type in ^{156}Dy, which has an axial shape at the moderate spins of interest in this communication.

For the first time, we apply the tidal wave concept to the γ vibration in a quantitative way. The traveling wave is described by cranking the triaxial potential about the long axis with the frequency ω_γ. The total angular momentum $J_3(\omega_\gamma,\gamma) = \langle 0|j_3|0\rangle$ and the total Routhian $E'(\omega_\gamma,\gamma)$ are calculated by means of the shell correction version of the cranking model as described in Ref. [45]. The total energy $E(J_3 = 2,\gamma) = E'(\omega_\gamma,\gamma) + \omega_\gamma J_3(\omega_\gamma,\gamma)$ is minimized with respect to γ, where ω_γ is fixed by requiring $J_3(\omega_\gamma,\gamma) = 2\hbar$.

The calculation is carried out for the vacuum configuration $|0,\omega_\gamma\rangle$, which corresponds to all negative energy quasiparticle Routhians being occupied. As for rotation about the short axes 1, 2 shown in Fig. 8, the continuation of the configuration to frequencies $\hbar\omega_\gamma > 0.3$ MeV leads into the region where the negative- and positive-energy quasiparticles encounter each other. The cranking model generates an unphysical mixing of the 0 configuration with high-j configurations (AB for example). In order to remove the mixing, the low-frequency Routhians are extrapolated using fourth-order polynomials, which corresponds to third-order perturbation theory with respect to ω_γ. The Harris parametrization,

$$J_3 = \omega_\gamma \mathcal{J}_0 + \omega_\gamma^3 \mathcal{J}_1, \quad E' = E_0 - \frac{\omega_\gamma}{2}\mathcal{J}_0 - \frac{\omega_\gamma^4}{4}\mathcal{J}_1, \quad (6)$$

is fitted to the cranking values in the range $0 \leqslant \hbar\omega_\gamma \leqslant 0.1$ MeV. The extrapolation very well reproduces the cranking calculations up to the region where the mixing with the high-j configurations sets in.

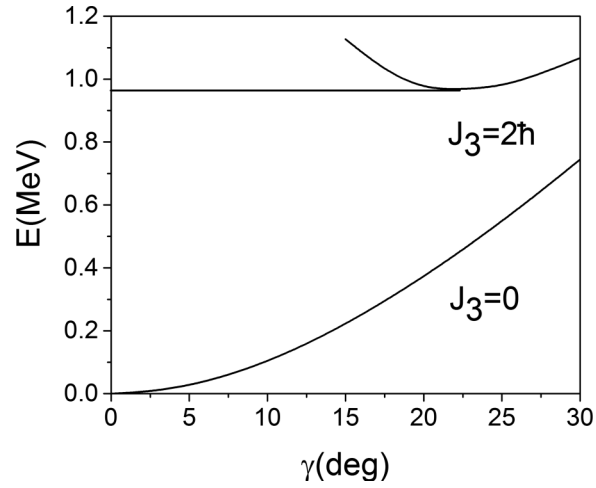

FIG. 12. Energies corresponding to angular momenta $J_3 = 0$ and $J_3 = 2\hbar$ calculated by the shell correction version of the cranking model.

Figure 12 shows that the energy with $J_3 = 0$ is minimal for $\gamma = 0$, which indicates that the γ band has the character of a tidal wave. For $J_3 = 2\hbar$ the minimum lies at $\gamma = 22.5^\circ$, which is the amplitude of the wave traveling about the symmetry axis. The energy of the minimum $E_\gamma = 0.97$ MeV is somewhat larger than the experimental energy of the γ bandhead of $E(2_2^+) = 0.890$ MeV. The energy $2\hbar\omega_\gamma = 0.91$ MeV, corresponding to angular velocity of the wave at the minimum of $\omega_\gamma = 0.456$ MeV/$\hbar$, remarkably well reproduces the experimental 2_2^+ energy. Up to spin $I = 10$ the coupling of the γ band to other bands is relatively weak. Accordingly, the bandhead energy is added to the g band in Fig. 9. Using the semiclassical expression given in Ref. [45], the cranking calculations provide the $B(E2,\omega)_{TAC}$ values. A rough estimate of the reduced transition probability $B(E2,2_2^+ \to 0_1^+)$ is given by the semiclassical expression for $J_3 = 1\hbar$, because the latter is proportional to J_3. The calculated ratio

$$\frac{B(E2,2_2^+ \to 0_1^+)}{B(E2,2_1^+ \to 0_1^+)} = \frac{B(E2,\omega_3(J_3 = 1\hbar)_{TAC}}{B(E2,\omega_1(J_1 = 2\hbar)_{TAC}} \quad (7)$$

of 0.043 is close to the experimental ratio of 0.048 [46].

The tidal wave approach reproduces the properties of γ-band head remarkably well without introducing any new parameters. This approach becomes equivalent to the QRPA approach when the two approaches are applied to the pairing + quadrupole quadrupole Hamiltonian and the linear extrapolation is used for $J_3(\omega_3)$ instead of the third-order Harris expression. The TPSM also describes the γ excitations by assuming a constant γ deformation. Instead of the semiclassical

cranking model it generates the traveling wave by means of quantal angular-momentum projection. The γ deformation is considered as a parameter that is adjusted to reproduce the excitation energy of the γ band on top of the ground-state band. The value of $\gamma = 20.6^\circ$ is close to 22.5° calculated by the tidal wave approach. As discussed above, this does not mean that ^{156}Dy has a rigid triaxial shape. As long as only the first excited γ band is of interest, there is no way to decide whether the triaxiality is static or dynamic. The wavelength of the first excitation is too large to resolve details of the potential in the γ degree of freedom that separate a harmonic traveling wave from a rigid rotor.

IV. CONCLUSIONS

The recently observed band structures in ^{156}Dy have been interpreted in the framework of the TPSM approach and QRPA based on the rotating mean field. The γ band built on the ground-state band is well reproduced by the TPSM, in particular the staggering pattern above $I = 10$, which within the collective model indicates the even-I-low pattern, corresponding to the γ-softness limit. The TPSM analysis strongly supports the interpretation proposed in the experimental work that two excited bands are the γ bands based on the neutron s band. This is the first detailed confirmation of γ bands based on the rotationally aligned two-quasineutron configurations, which have been suggested in the framework of QRPA. It would be quite interesting to apply the recently developed state-of-the-art approaches [47–50] to investigate the γ bands built on the quasiparticle excitations.

ACKNOWLEDGMENTS

S.J. would like to acknowledge MHRD (Govt. of India) for providing the financial support to carry out the research work. Two of us (S.N.T.M. and J.F.S.-S.) would like to acknowledge grants from the National Research Foundation (NRF) of South Africa. S.F. acknowledges support by the U.S. Department of Energy, Grant No. DE-FG02-95ER4093.

[1] A. Bohr and B. R. Mottelson, *Nuclear Structure*, Vol. II (Benjamin, New York, 1975).
[2] J. D. Morrison *et al.*, Europhys. Lett. **6**, 493 (1988).
[3] J. Simpson *et al.*, J. Phys. G **13**, 235 (1987).
[4] F. G. Kondev *et al.*, Phys. Lett. B **437**, 35 (1998).
[5] J. Ollier, J. Simpson, M. A. Riley, E. S. Paul, X. Wang, A. Aguilar, M. P. Carpenter, I. G. Darby, D. J. Hartley, R. V. F. Janssens, F. G. Kondev, T. Lauritsen, P. J. Nolan, M. Petri, J. M. Rees, S. V. Rigby, C. Teal, J. Thomson, C. Unsworth, S. Zhu, A. Kardan, and I. Ragnarsson, Phys. Rev. C **83**, 044309 (2011).
[6] S. N. Majola, D. J. Hartley, L. L. Riedinger, J. F. Sharpey-Schafer, J. M. Allmond, C. Beausang, M. P. Carpenter, C. J. Chiara, N. Cooper, D. Curien, B. J. P. Gall, P. E. Garrett, R. V. F. Janssens, F. G. Kondev, W. D. Kulp, T. Lauritsen, E. A. McCutchan, D. Miller, J. Piot, N. Redon, M. A. Riley, J. Simpson, I. Stefanescu, V. Werner, X. Wang, J. L. Wood, C. H. Yu, and S. Zhu, Phys. Rev. C **91**, 034330 (2015).
[7] V. G. Soloviev and N. Yu. Shirikova, Z. Phys. A **301**, 263 (1981).
[8] V. G. Soloviev, *Theory of Atomic Nuclei: Quasiparticles and Phonons* (Institute of Physics, London, 1992).
[9] J. Leandri and R. Piepenbring, Phys. Rev. C **37**, 2779 (1988).
[10] M. K. Jammari and R. Piepenbring, Nucl. Phys. A **487**, 77 (1988).
[11] H. G. Borner and J. Joli, J. Phys. **G 19**, 217 (1993).
[12] D. G. Burke and P. C. Sood, Phys. Rev. C **51**, 3525 (1995).
[13] K. Kumar, *Nuclear Models and Search for Unity in Nuclear Physics* (Universitetforlaget, Bergen, Norway, 1984).
[14] Y. R. Shimizu and K. Matsuyanagi, Prog. Theor. Phys. **67**, 1637 (1982).
[15] Y. R. Shimizu and K. Matsuyanagi, Prog. Theor. Phys. **67**, 1641 (1982).
[16] Y. R. Shimizu and K. Matsuyanagi, Prog. Theor. Phys. **70**, 144 (1982).
[17] Y. R. Shimizu and K. Matsuyanagi, Prog. Theor. Phys. **72**, 799 (1982).
[18] J. Kvasil and R. G. Nazmitdinov, Phys. Rev. C **69**, 031304(R) (2004).
[19] J. Kvasil and R. G. Nazmitdinov, Phys. Lett. B **650**, 331 (2007).
[20] R. G. Nazmitdinov and J. Kvasil, J. Exp. Theor. Phys. **105**, 962 (2007).
[21] S. Jehangir, G. H. Bhat, J. A. Sheikh, R. Palit, and P. A. Ganai, Nucl. Phys. A **968**, 48 (2017).
[22] J. Marcellino, E. H. Wang, C. J. Zachary, J. H. Hamilton, A. V. Ramayya, G. H. Bhat, J. A. Sheikh, A. C. Dai, W. Y. Liang, F. R. Xu, J. K. Hwang, N. T. Brewer, Y. X. Luo, J. O. Rasmussen, S. J. Zhu, G. M. Ter-Akopian, and Y. T. Oganessian, Phys. Rev. C **96**, 034319 (2017).
[23] R. Palit, G. H. Bhat, and J. A. Sheikh, Eur. Phys. J. A **53**, 90 (2017).
[24] A. Navin, M. Rejmund, S. Bhattacharyya, R. Palit, G. H. Bhat, J. A. Sheikh, A. Lemasson, S. Bhattacharya, M. Caamaño, E. Clément, O. Delaune, F. Farget, G. de France, and B. Jacquot, Phys. Lett. B **767**, 480 (2017).
[25] J. A. Sheikh, G. H. Bhat, W. A. Dar, S. Jehangir, and P. A. Ganai, Phys. Scr. **91**, 063015 (2016).
[26] G. H. Bhat, J. A. Sheikh, Y. Sun, and R. Palit, Nucl. Phys. A **947**, 127 (2016).
[27] J. A. Sheikh and K. Hara, Phys. Rev. Lett. **82**, 3968 (1999).
[28] J. A. Sheikh, G. H. Bhat, Y. Sun, G. B. Vakil, and R. Palit, Phys. Rev. C **77**, 034313 (2008).
[29] J. A. Sheikh, G. H. Bhat, R. Palit, Z. Naik, and Y. Sun, Nucl. Phys. A **824**, 58 (2009).
[30] K. Hara and Y. Sun, Int. J. Mod. Phys. E **4**, 637 (1995).
[31] L.-J. Wang, Y. Sun, T. Mizusaki, M. Oi, and S. K. Ghorui, Phys. Rev. C **93**, 034322 (2016).
[32] L.-J. Wang, F.-Q. Chen, T. Mizusaki, M. Oi, and Y. Sun, Phys. Rev. C **90**, 011303 (2014).
[33] G. H. Bhat, W. A. Dar, J. A. Sheikh, and Y. Sun, Phys. Rev. C **89**, 014328 (2014).
[34] J. A. Sheikh, G. H. Bhat, Y.-X. Liu, F.-Q. Chen, and Y. Sun, Phys. Rev. C **84**, 054314 (2011).
[35] G. H. Bhat, J. A. Sheikh, Y. Sun, and U. Garg, Phys. Rev. C **86**, 047307 (2012).

[36] Y. Sun, K. Hara, J. A. Sheikh, J. G. Hirsch, V. Velazquez, and M. Guidry, Phys. Rev. C **61**, 064323 (2000).
[37] S. Raman, C. H. Malarkey, W. T. Milner, C. W. Nestor Jr., and P. H. Stelson, At. Data Nucl. Data Tables **36**, 1 (1987).
[38] O. Moller, A. Dewald, P. Petkov, B. Saha, A. Fitzler, K. Jessen, D. Tonev, T. Klug, S. Heinze, J. Jolie, P. vonBrentano, D. Bazzacco, C. A. Ur, E. Farnea, M. Axiotis, S. Lunardi, G. de Angelis, D. R. Napoli, N. Marginean, T. Martinez, M. A. Caprio, and R. F. Casten, Phys. Rev. C **74**, 024313 (2006).
[39] A. Dewald *et al.*, Eur. Phys. J. A **20**, 173 (2004).
[40] P. Petkov *et al.*, Phys. Rev. C **68**, 034328 (2003).
[41] S. Frauendorf, Int. J. Mod. Phys. E **24**, 1541001 (2015).
[42] R. Bengtsson and S. Frauendorf, Nucl. Phys. A **327**, 139 (1979).
[43] S. Frauendorf, Y. Gu, and J. Sun, Int. J. Mod. Phys. E **20**, 465 (2011).
[44] A. D. Ayangeakaa *et al.*, Phys. Rev. Lett. **110**, 102501 (2013).
[45] S. Frauendorf, Nucl. Phys. A **677**, 115 (2000).
[46] National Nuclear Data Center, Brookhaven National Laboratory, http://www.nndc.bnl.gov
[47] J. L. Egido, M. Borrajo, and T.-R. Rodriguez, Phys. Rev. Lett. **116**, 052502 (2016).
[48] Y. Utsuno, N. Shimizu, T. Otsuka, T. Yoshida, and Y. Tsunoda, Phys. Rev. Lett. **114**, 032501 (2015).
[49] Y. F. Niu, Z. M. Niu, G. Colo, and E. Vigezzi, Phys. Rev. Lett. **114**, 142501 (2015).
[50] K. Nomura, T. Niksic, and D. Vretenar, Phys. Rev. C **93**, 054305 (2016).